Discriminator-free Unsupervised Domain Adaptation for Multi-label Image Classification

Inder Pal Singh[1], Enjie Ghorbel[12], Anis Kacem[1], Arunkumar Rathinam[1], Djamila Aouada[1]

[1]Interdisciplinary Centre for Security, Reliability and Trust (SnT), University of Luxembourg, Luxembourg
[2]High Institute of Multimedia Arts (ISAMM), University of Manouba, Tunisia

{inder.singh, enjie.ghorbel, anis.kacem, arunkumar.rathinam, djamila.aouada}@uni.lu

Abstract

In this paper, a discriminator-free adversarial-based Unsupervised Domain Adaptation (UDA) for Multi-Label Image Classification (MLIC) referred to as DDA-MLIC is proposed. Recently, some attempts have been made for introducing adversarial-based UDA methods in the context of MLIC. However, these methods, which rely on an additional discriminator subnet present one major shortcoming. The learning of domain-invariant features may harm their task-specific discriminative power, since the classification and discrimination tasks are decoupled. Herein, we propose to overcome this issue by introducing a novel adversarial critic that is directly deduced from the task-specific classifier. Specifically, a two-component Gaussian Mixture Model (GMM) is fitted on the source and target predictions in order to distinguish between two clusters. This allows extracting a Gaussian distribution for each component. The resulting Gaussian distributions are then used for formulating an adversarial loss based on a Fréchet distance. The proposed method is evaluated on several multi-label image datasets covering three different types of domain shift. The obtained results demonstrate that DDA-MLIC outperforms existing state-of-the-art methods in terms of precision while requiring a lower number of parameters. The code is publicly available at github.com/cvi2snt/DDA-MLIC.[1]

1. Introduction

Multi-Label Image Classification (MLIC) aims at predicting the presence/absence of a set of objects in a given
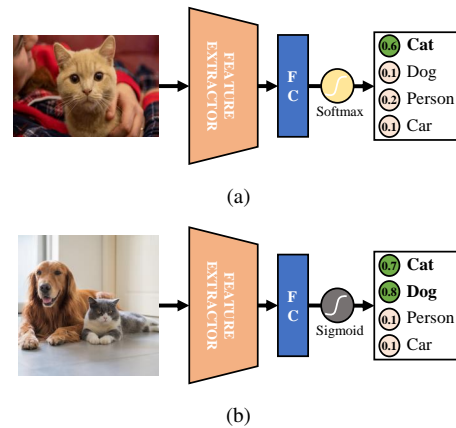

Figure 1. The work of [4] cannot be directly applied to MLIC due to the differences between the two tasks: (a) Single-label image classification uses a softmax activation function to convert the predicted logits into probabilities such that the sum of all class probabilities is equal to one; and (b) On the other hand, multi-label image classification uses sigmoid activation where each logit is scaled between 0 and 1, giving higher probability values for the objects present in an image.

image. It is widely studied in the Computer Vision community due to its numerous fields of applications such as object recognition [2], scene classification [25], and attribute recognition [14, 28]. With the latest advancements in deep learning, several MLIC methods [10, 21, 22, 29] have achieved remarkable performance on well-known datasets [8, 16]. Nevertheless, the effectiveness of deep learning-based methods widely relies on the availability of annotated datasets. This requires costly and time-consuming efforts. As a result, given the limited number of labeled data, existing MLIC methods tend to have poor generalization capabilities to unseen domains. This problem is commonly known as *domain-shift*, where a method trained on a *source* dataset fails to generalize on a *target*

one belonging to a different domain. To overcome this issue, *Unsupervised Domain Adaptation (UDA)* [9, 19] can be an interesting strategy. The idea behind UDA is to leverage unlabeled data from the target dataset to reduce the gap between the source and the target domains.

In the literature, many works have been proposed for UDA in the context of single-label image classification [9, 17–19, 23], while less efforts have been dedicated to proposing UDA methods that are suitable for MLIC. Inspired by the predominance of adversarial-based approaches in single-label image classification, few methods [15, 20, 27] have attempted to extend UDA to MLIC. Similar to [9], these adversarial approaches leverage a domain discriminator for implicitly reducing the domain gap. In particular, a min-max two-player game guides the generator to extract domain-invariant features that fool the discriminator. Nevertheless, this may come at the cost of decreasing their task-specific discriminative power, as highlighted in [4].

Chen et al. [4] attempted to solve this problem in the context of single-label image classification by implicitly reusing the classifier as a discriminator. In particular, they considered the difference between inter-class and intra-class correlations of the classifier probability predictions as an adversarial critic. Nevertheless, the per-class prediction probabilities are not linearly dependent in the context of MLIC. This means that these probabilities are not constrained to sum up to one, as shown in Figure 1. Hence, the approach of [4] can only be naively generalized to MLIC by considering multiple binary classifiers, namely, one for each label. Therefore, a critic similar to the one in [4] can be used by computing the correlations between the probability predictions of each binary classifier. However, this is not optimal since the domain adaptation would be carried out for each label classifier separately, ignoring the correlations between the different labels. This is also experimentally confirmed in Section 4.

In this paper, we introduce a discriminator-free adversarial UDA approach for MLIC based on a novel adversarial critic. As in [4], we propose to leverage the task-specific classifier for defining the adversarial critic. However, instead of relying on the prediction correlations, which is not suitable in the case of MLIC, we propose to cluster the probability predictions into two sets (one in the neighborhood of 0 and another one in the neighborhood of 1), estimate their respective distributions and define the critic as the distance between the estimated distributions from the source and target data. This intuition comes from the fact that source data are usually more confidently classified (as positive or negative) than target ones, as illustrated in Figure 2. The same figure also highlights that the distribution of predictions can be modeled by two clusters; showing the interest of modelling the predictions with a bimodal distribution. Hence, we assume that the distribution shape of
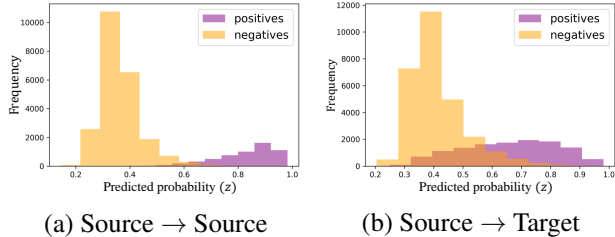

(a) Source $\rightarrow$ Source (b) Source $\rightarrow$ Target

Figure 2. Histogram of classifier predictions[2]. Predicted probabilities using source-only trained classifier[2] on: (a) source dataset[3] ($\mathcal{I}_s$), and (b) target dataset[3] ($\mathcal{I}_t$).

probability predictions can be used to implicitly discriminate source and target data. Concretely, we propose to fit a Gaussian Mixture Model (GMM) with two components on both the source and target predictions. A Fréchet distance [7] between the estimated pair of components is then used to define the proposed discrepancy measure. The experimental results show that the proposed approach outperforms state-of-the-art methods in terms of mean Average Precision (mAP) while significantly reducing the number of network parameters.

In summary, our contributions are:

- A novel domain discrepancy for multi-label image classification based on the distribution of the task-specific classifier predictions;

- An effective and efficient adversarial unsupervised domain adaptation method for multi-label image classification. The proposed adversarial strategy does not require an additional discriminator, hence reducing the network size during training;

- An experimental quantitative and qualitative analysis on several benchmarks showing that the proposed method outperforms state-of-the-art works.

The rest of the paper is organized as follows. Section 2 formulates the problem of domain adaptation for multi-label image classification, and presents our intuition behind using the classifier as a critic. Section 3 introduces the proposed approach termed DDA-MLIC. The experimental results are reported and discussed in Section 4. Finally, Section 5 concludes this work and draws some perspectives.

2. Problem Formulation and Motivation

2.1. Problem formulation

Let $\mathcal{D}_s = (\mathcal{I}_s, \mathcal{Y}_s)$ and $\mathcal{D}_t = (\mathcal{I}_t, \mathcal{Y}_t)$ be the source and target datasets, respectively, with P_s and P_t being their re-

---

[2]TResNet-M [22] trained on UCM [3] dataset.
[3]Source: UCM [3] validation set (420 images), Target: AID [12] validation set (600 images).

spective probability distributions such that $P_s \neq P_t$. Let us assume that they are both composed of N object labels. Note that $\mathcal{I}_s = \{\mathbf{I}_s^k\}_{k=1}^{n_s}$ and $\mathcal{I}_t = \{\mathbf{I}_t^k\}_{k=1}^{n_t}$ refer to the sets of n_s source and n_t target image samples, respectively, while $\mathcal{Y}_s = \{\mathbf{y}_s^k\}_{k=1}^{n_s}$ and $\mathcal{Y}_t = \{\mathbf{y}_t^k\}_{k=1}^{n_t}$ are their associated sets of labels.

Let us denote by $\mathcal{I}$ the set of all images such that $\mathcal{I} = \mathcal{I}_s \cup \mathcal{I}_t$. Given an input image $\mathbf{I} \in \mathcal{I}$ with $\mathbf{y} \in \{0, 1\}^N$ being its label, the goal of *unsupervised domain adaptation* for *multi-label image classification* is to estimate a function $f : \mathcal{I} \mapsto \{0, 1\}^N$ such that,

$$f(\mathbf{I}) = \mathbb{1}_{f_c \circ f_g(\mathbf{I}) > \tau} = \mathbb{1}_{\mathbf{Z} > \tau} = \mathbf{y}, \quad (1)$$

where $f_g : \mathcal{I} \mapsto \mathbb{R}^d$ extracts d-dimensional features, $f_c : \mathbb{R}^d \mapsto [0, 1]^N$ predicts the probability of object presence, $\mathbf{Z} = f_c \circ f_g(\mathbf{I}) \in [0, 1]^N$ corresponds to the predicted probabilities, $\mathbb{1}$ is an indicator function, $>$ is a comparative element-wise operator with respect to a chosen threshold τ. Note that only $\mathcal{D}_s$ and $\mathcal{I}_t$ are used for training. In other words, the target dataset is assumed to be unlabeled.

To achieve this goal, some existing methods [15] have adopted an adversarial strategy by considering an additional discriminator f_d that differentiates between source and target data. Hence, the model is optimized using a classifier loss $\mathcal{L}_c$ such as the asymmetric loss (ASL) [21] and an adversarial loss $\mathcal{L}_{adv}$ defined as,

$$\begin{aligned} \mathcal{L}_{adv} = \mathbb{E}_{f_g(\mathbf{I}_s) \sim \bar{P}_s} \log \frac{1}{f_d(f_g(\mathbf{I}_s))} + \\ \mathbb{E}_{f_g(\mathbf{I}_t) \sim \bar{P}_t} \log \frac{1}{(1 - f_d(f_g(\mathbf{I}_t)))}, \end{aligned} \quad (2)$$

where $\bar{P}_s$ and $\bar{P}_t$ are the distributions of the learned features from source and target samples $\mathcal{I}_s$ and $\mathcal{I}_t$, respectively.

While the adversarial paradigm has shown great potential [15], the use of an additional discriminator f_d which is decoupled from f_c may lead to mode collapse as discussed in [4]. Inspired by the same work, we aim at addressing the following question – *Could we leverage the outputs of the task-specific classifier $f_c \circ f_g$ in the context of multi-label classification for implicitly discriminating the source and the target domains?*

2.2. Motivation: domain discrimination using the distribution of the classifier output

The goal of MLIC is to identify the classes that are present in an image (*i.e.*, *positive labels*) and reject the ones that are not present (*i.e.*, *negative labels*). Hence, the classifier f_c is expected to output high probability values for the positive labels and low probability values for the negative ones. Formally, let $z = \theta(f_c(f_g(\mathbf{I}))) = \theta(\mathbf{Z}) \sim \hat{P}$ be the random variable modelling the predicted probability of any

class and $\hat{P}$ its probability distribution, with θ being a uniform random sampling function that returns the predicted probability of a randomly selected class. In general, a well-performing classifier is expected to classify confidently both negative and positive samples. Ideally, this would mean that the probability distribution $\hat{P}$ should be formed by two clusters with low variance in the neighborhood of 0 and 1, respectively denoted by $\mathcal{C}_0$ and $\mathcal{C}_1$. Hence, our hypothesis is that a drop in the classifier performance due to a domain shift can be reflected in $\hat{P}$.

Let $z_s = \theta(f_c(f_g(\mathbf{I}_s))) \sim \hat{P}_s$ and $z_t = \theta(f_c(f_g(\mathbf{I}_t))) \sim \hat{P}_t$ be the random variables modelling the predicted probability obtained from the source and target data and $\hat{P}_s$ and $\hat{P}_t$ be their distributions, respectively. Concretely, we propose to investigate whether the shift between the source and target domains is translated in $\hat{P}_s$ and $\hat{P}_t$. If a clear difference is observed between $\hat{P}_s$ and $\hat{P}_t$, this would mean that the classifier f_c should be able to discriminate between source and target samples. Thus, this would allow the definition of a suitable critic directly from the classifier predictions.

To support our claim, we trained a model[4] f using the labelled source data $\mathcal{D}_s$ without involving the target images[5] $\mathcal{I}_t$. In Figure 2 (a), we visualize the histogram of the classifier probability outputs when the model is tested on the source domain. It can be clearly observed that the predicted probabilities on the source domain, denoted by z_s, can be grouped into two separate clusters. Figure 2 (b) shows the same histogram when the model is tested on target samples. In contrast to the source domain, the classifier probability outputs, denoted by z_t, are more spread out in the target domain. In particular, the two clusters are less separable than in the source domain. This is due to the fact that the classifier f_c benefited from the supervised training on the source domain, and as a result it gained an implicit discriminative ability between the source and target domains.

Motivated by the observations discussed above, we propose to reuse the classifier to define a critic function based on $\hat{P}_s$ and $\hat{P}_t$. In what follows, we describe our approach including the probability distribution modelling ($\hat{P}_s$ and $\hat{P}_t$) and the adversarial strategy for domain adaptation.

3. An Implicit Multi-Label Domain Adaptation Adversarial Strategy

As discussed in Section 2.2, the classifier probability predictions are usually formed by two clusters with nearly Gaussian distributions. Consequently, as shown in Figure 3 (a), we propose to approximate the distributions $\hat{P}_s$ and $\hat{P}_t$ by a two-component Gaussian Mixture Model (GMM) as

---

[4]TResNet-M [22] trained on UCM [3] dataset.
[5]Source: UCM [3] validation set (420 images), Target: AID [12] validation set (600 images).

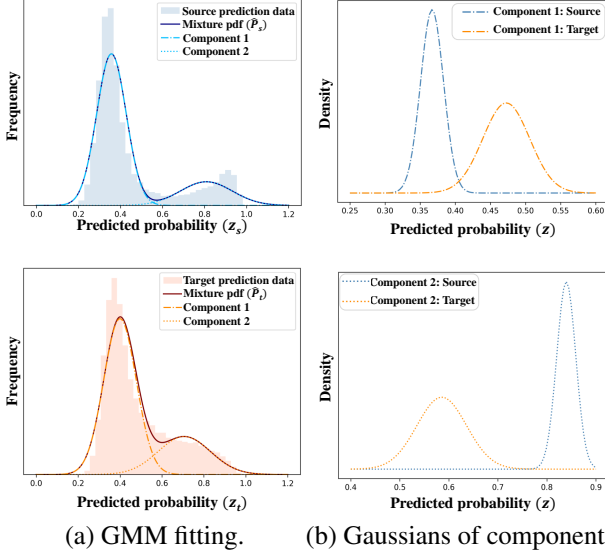(a) GMM fitting.   (b) Gaussians of components.

Figure 3. (a) The classifier[6] predictions z_s and z_t for both source and target datasets[7], respectively, can be grouped into two clusters. Hence, a two-component GMM can be fitted for both source ($\hat{P}_s$) and target ($\hat{P}_t$). While the first component is close to 0, the second is close to 1, (b) A component-wise comparison between source ($\hat{P}_s^1, \hat{P}_s^2$) and target ($\hat{P}_t^1, \hat{P}_t^2$) Gaussians of distributions extracted from the fitted GMM confirms that target predictions are likely to be farther from 0 and 1 with a higher standard deviation than the source.

follows,

$$\hat{P}_s(z_s) \approx \sum_{i=1}^{2} \pi_i^s \mathcal{N}(z_s|\mu_i^s, \sigma_i^s) \,, \qquad (3)$$

and,

$$\hat{P}_t(z_t) \approx \sum_{i=1}^{2} \pi_i^t \mathcal{N}(z_t|\mu_i^t, \sigma_i^t) \,, \qquad (4)$$

where $\mathcal{N}(z_t|\mu_i^t, \sigma_i^t)$ denotes the i-th Gaussian distribution, with the mean μ_i^t and the variance σ_i^t, fitted on the target predicted probabilities z_t and π_i^t its mixture weight such that $\pi_1^t + \pi_2^t = 1$. Similarly, $\mathcal{N}(z_s|\mu_i^s, \sigma_i^s)$ denotes the i-th Gaussian distribution, with the mean μ_i^s and the variance σ_i^s, fitted on the source predicted probabilities z_s and π_i^s its mixture weight such that $\pi_1^s + \pi_2^s = 1$.

An Expectation-Maximization (EM) algorithm is used to estimate the GMM parameters. In both source and target domains, we assume that the first component of the GMM corresponds to the cluster $\mathcal{C}_0$ (with a mean close to 0), while the second corresponds to $\mathcal{C}_1$ (with a mean close to 1).

However, due to a large number of negative predictions as compared to positive ones, the component $\mathcal{C}_0$ tends to be more dominant. In fact, in a given image, only few objects are usually present from the total number of classes. To alleviate this phenomenon, we propose to extract two Gaussian

components from the source and target GMM, ignoring the estimated weights illustrated in Figure 3 (b).

Hence, we propose to redefine the adversarial loss $\mathcal{L}_{adv}$ by computing a Fréchet distance d_F [7] between each pair of source and target components from a given cluster as follows.

$$\mathcal{L}_{adv} = \sum_{i=1}^{2} \alpha_i d_F(\mathcal{N}(z_t|\mu_i^t, \sigma_i^t), \mathcal{N}(z_s|\mu_i^s, \sigma_i^s)) \,, \qquad (5)$$

with α_i weights that are empirically fixed. Since the computed distributions are univariate Gaussians, the Fréchet distance between two distributions, also called the 2-Wasserstein (2W) distance, is chosen as it can be explicitly computed as follows,

$$d_F^2(\mathcal{N}(z_1|\mu_1, \sigma_1), \mathcal{N}(z_2|\mu_2, \sigma_2)) = (\mu_1 - \mu_2)^2 + (\sigma_1 - \sigma_2)^2, \qquad (6)$$

where $\mathcal{N}(z_1|\mu_1, \sigma_1)$ and $\mathcal{N}(z_2|\mu_2, \sigma_2)$ are two Gaussians with a mean of μ_1 and μ_2 and a standard deviation of σ_1 and σ_2, respectively. In addition, compared to the commonly used 1-Wasserstein (1W) distance, it considers second-order moments. Finally, in [1], the 2W distance has been demonstrated to have nicer properties e.g., continuity and differentiability, for optimizing neural networks as compared to other divergences and distances between two distributions such as the Kullback-Leibler (KL) divergence and the Jensen-Shannon (JS) divergence. The relevance of the 2W distance is further discussed in Section 4.9.

The overall architecture of the proposed method is shown in Figure 4. Similar to [4], our network consists of a feature extractor f_g that aims to extract discriminative image features from source $\mathcal{D}_s$ and target $\mathcal{I}_t$ datasets and a classifier f_c that simultaneously performs the classification and discriminates between source and target features by minimizing the proposed adversarial loss $\mathcal{L}_{adv}$. A Gradient Reversal Layer (GRL) between f_g and f_c enforces the feature extractor to fool the classifier when acting as a discriminator, hence implicitly learning domain-invariant features.

4. Experiments

4.1. Datasets

In our experiments, different types of domain gaps are considered. Due to the limited availability of multi-label domain adaptation datasets, we convert several object detection and semantic segmentation datasets for the task of MLIC.

---

[6]TResNet-M [22] trained on UCM [3] dataset.
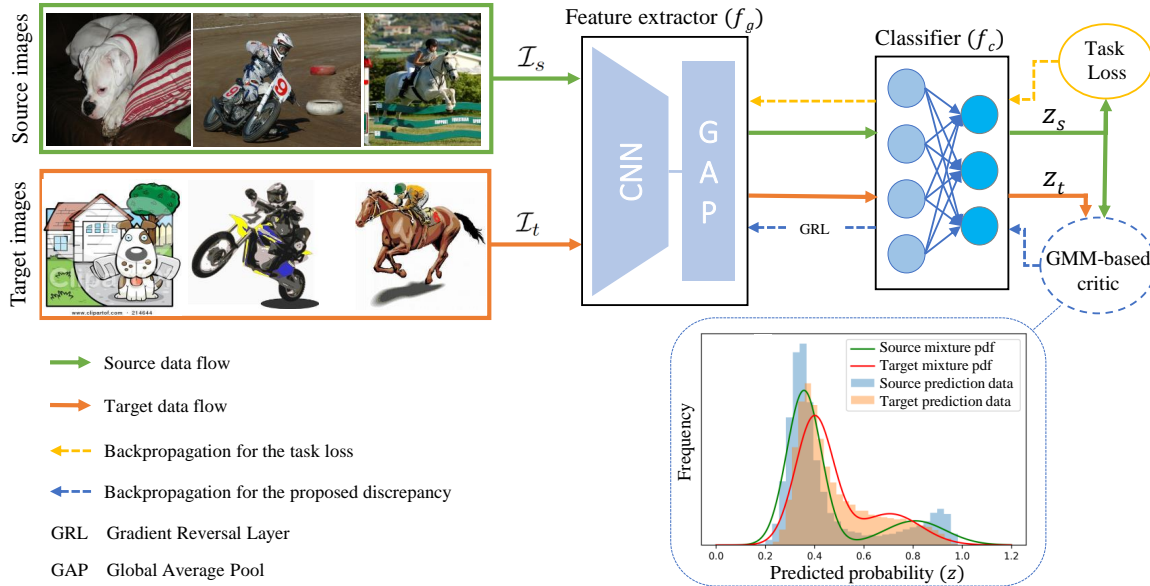[7]Source: UCM [3] validation set (420 images), Target: AID [12] validation set (600 images).

Figure 4. Overall proposed architecture of DDA-MLIC: The feature extractor (f_g) learns discriminative features from source and target images. The task classifier (f_c) performs two actions simultaneously: 1) it learns to classify source samples correctly using a supervised task loss, and 2) when used as a discriminator, it aims to minimize/maximize the proposed discrepancy between source and target predictions.

Cross-sensor domain shift Similar to [15], we use three multi-label aerial image datasets that have been captured using different sensors resulting in different resolutions, pixel densities and altitudes, namely: 1) **AID** [12] multi-label dataset was created from the original multi-class AID dataset [30] by labelling 3000 aerial images, including 2400 for training and 600 for testing, with a total of 17 categories. 2) **UCM** [3] multi-label dataset was recreated from the original multi-class classification dataset [31] with a total of 2100 image samples containing the same 17 object labels as AID. We randomly split the dataset into training and testing sets with 2674 and 668 image samples, respectively. 3) **DFC** [11] multi-label dataset provides 3342 high resolution images with training and testing splits of, respectively, 2674 and 668 samples labelled from a total of 8 categories. In our experiments, the 6 common categories between DFC and the other two benchmarks are used.

Sim2real domain shift We use the following two datasets to investigate the domain gap between real and synthetic scene understanding images. 1) **PASCAL-VOC** [8] is one of the most widely used real image datasets for MLIC with more than $10K$ image samples. It covers 20 object categories. The training and testing sets contain 5011 and 4952 image samples, respectively. 2) **Clipart1k** [13] provides 1000 synthetic clipart image samples, annotated with 20 object labels, similar to VOC. Since it is proposed for the task of object detection, we make use of the category labels for

bounding boxes to create a multi-label version. Half of the data are used for training and the rest is used for testing.

Cross-weather domain shift In order to study the domain shift caused by different weather conditions, two widely used urban street datasets have been used, namely: 1) **Cityscapes** [6] which is introduced for the task of semantic image segmentation and consists of 5000 real images captured in daytime. 2) **Foggy-cityscapes** [24] which is a synthesized version of Cityscapes where an artificial fog is introduced. We generate a multi-label version of these datasets for the task of MLIC considering only 11 categories out of the original 19 to avoid including the objects that appear in all the images.

4.2. Implementation details

The proposed DDA-MLIC makes use of the TResNet-M [22] as a backbone and the Asymmetric Loss (ASL) [21] as the task loss. All the methods are trained using the Adam optimizer with a cosine decayed maximum learning rate of 10^{-3}. For all the experiments, we make use of NVIDIA TITAN V with a batch size of 64 for a total of 25 epochs or until convergence. The input image resolution has been fixed to 224×224..

4.3. Baselines

To evaluate the proposed approach, we consider standard MLIC approaches, namely, ResNet [10], ML-GCN [5],

Table 1. Cross-sensor domain shift: Comparison with the state-of-the-art in terms of number of model parameters (in millions), and % scores of mAP, per-class averages (CP, CR, CF1) and overall averages (OP, OR, OF1) for aerial image datasets. Two settings are considered, *i.e.*, AID → UCM and UCM → AID. Best results are highlighted in **bold**.

Type	Method	# params	AID → UCM							UCM → AID						
			mAP	P_C	R_C	F_C	P_O	R_O	F_O	mAP	P_C	R_C	F_C	P_O	R_O	F_O
MLIC	ResNet101 [10]	42.5	57.5	**60.0**	47.5	47.0	69.1	71.5	**70.3**	51.7	50.6	29.6	33.9	88.0	48.5	62.5
	ML-GCN [5]	44.9	53.7	55.3	44.3	45.9	70.2	68.7	69.4	51.3	50.1	29.9	34.0	88.0	49.7	63.6
	ML-AGCN [26]	36.6	55.2	36.6	**64.9**	45.1	45.0	**88.1**	59.6	52.1	48.2	**47.4**	**42.9**	77.1	**79.8**	**78.4**
	ASL (TResNetM) [21]	**29.4**	55.4	48.7	52.8	47.1	58.7	79.1	67.4	54.1	54.5	40.2	41.9	85.4	65.1	73.9
Disc.-based	DANN (TResNetM+ASL) [9]	**29.4**	52.5	59.1	31.6	36.3	**70.9**	53.7	61.1	51.6	52.1	23.2	27.9	83.2	27.8	41.7
	DA-MAIC (TResNetM+ASL) [15]	36.6	54.4	55.3	37.5	38.6	68.0	67.9	67.9	50.5	51.8	22.9	29.0	91.6	35.2	50.8
Disc.-free	DALN (TResNetM+ASL) [4]	**29.4**	53.1	53.3	32.4	36.7	69.2	53.9	60.6	53.2	52.2	29.3	32.7	82.0	41.2	54.8
	DDA-MLIC (ours)	**29.4**	**63.2**	52.5	63.7	**55.1**	59.4	82.8	69.2	**54.9**	53.9	30.4	35.5	84.6	41.0	55.3

Table 2. Cross-sensor domain shift: Comparison with the state-of-the-art in terms of number of model parameters (in millions), and % scores of mAP, per-class averages (CP, CR, CF1) and overall averages (OP, OR, OF1) for aerial image datasets. Two settings are considered, *i.e.*, AID → DFC and UCM → DFC. Best results are highlighted in **bold**.

Type	Method	# params	AID → DFC							UCM → DFC						
			mAP	P_C	R_C	F_C	P_O	R_O	F_O	mAP	P_C	R_C	F_C	P_O	R_O	F_O
MLIC	ResNet101 [10]	42.5	56.9	52.9	61.5	48.7	46.1	63.7	53.5	66.4	74.4	31.2	36.9	67.2	37.2	47.9
	ML-GCN [5]	44.9	58.9	**56.7**	57.9	45.8	45.7	65.0	53.7	64.6	72.4	32.0	35.6	64.4	38.9	48.5
	ML-AGCN [26]	36.6	51.6	41.5	**83.8**	52.3	40.2	**88.7**	55.3	70.3	68.4	**56.1**	47.8	53.8	**58.5**	56.0
	ASL (TResNetM) [21]	**29.4**	56.1	49.6	68.4	49.9	43.5	74.1	54.8	68.9	66.3	53.1	44.0	52.6	57.0	54.7
Disc.-based	DANN (TResNetM+ASL) [9]	**29.4**	43.0	40.7	13.6	19.3	46.0	15.6	23.3	64.1	77.3	22.6	30.1	68.6	26.5	38.2
	DA-MAIC (TResNetM+ASL) [15]	36.6	55.4	49.8	60.4	44.7	47.3	64.1	54.4	65.8	71.4	39.3	39.7	59.9	44.6	51.1
Disc.-free	DALN (TResNetM+ASL) [4]	**29.4**	44.7	43.7	23.8	27.6	**48.9**	27.4	35.1	65.6	**82.6**	21.3	32.0	**75.2**	22.1	34.1
	DDA-MLIC (ours)	**29.4**	**62.1**	47.6	75.5	**55.3**	48.9	76.2	**59.6**	**70.6**	67.2	55.7	**49.3**	55.0	58.4	**56.6**

ML-AGCN [26] and ASL [21] as well the recently introduced DA method for MLIC approach called DA-MAIC [15]. Note that the standard MLIC approaches are trained on source-only datasets, hence do not incorporate any domain adaptation strategy. In addition, given that the problem of DA for MLIC is under-explored, we propose to adapt two additional DA methods for single-label classification to MLIC. In particular, the existing discriminator-based and discriminator-free adversarial DA approaches i.e., DANN [9] and DALN [4] are considered by adopting the following changes. The original cross entropy loss in both DANN and DALN is replaced with the Asymmetric Loss (ASL) [21]. Additionally, we propose to convert the multi-label output of the classifier in DALN to multiple binary predictions before applying the Nuclear Wasserstein Discrepancy (NWD) [4]. Moreover, for a fair comparison, we replace the CNN backbone from the conventional ResNet101 to the same backbone as ours, namely TResNet-M [22], for the three DA baselines.

4.4. Experimental settings

In our experiments, we report the number of model parameters, mean Average Precision (mAP), average per-Class Precision (CP), average per-Class Recall (CR), average per-Class F1-score (CF1), average Overall Precision (OP), average overall recall (OR) and average Overall F1-score (OF1). Given the seven considered datasets, *i.e.*, AID, UCM, DFC, VOC, Clipart, Cityscapes and Foggyc-

ityscapes, seven experimental settings are considered, *i.e.*, AID → UCM, UCM → AID, AID → DFC, UCM → DFC, VOC → Clipart, Clipart → VOC, Cityscapes → Foggy. For instance, AID → UCM indicates that during the training AID is fixed as the source dataset while UCM is considered as the target one. The results are reported on the testing set of the target dataset.

4.5. Results

4.5.1 Quantitative analysis

Table 1, Table 2, Table 3 and Table 4 quantitatively compare the proposed approach to state-of-the-art methods. It can be seen that our model requires equal or fewer number of parameters than other state-of-the-art works, with a total number of 29.4 million parameters. We achieve the best performance in terms of mAP for AID → UCM, UCM → AID, AID → DFC, UCM → DFC, Clipart → VOC and Cityscapes → Foggy.

The first 4 rows of Table 1, Table 2, Table 3 and Table 4 report the obtained results using different methods of MLIC without DA [5, 10, 21, 26]. It can be observed that our method consistently outperforms all these methods in all settings (cross-sensor, sim2Real, and cross-weather) in terms of mAP showing the effectiveness of the proposed DA method for MLIC.

Furthermore, the results reported in the 5th and 6th rows of Table 1, Table 2, Table 3, Table 4 show that the proposed discriminator-free DA method clearly outper-

Table 3. Sim2Real domain shift: Comparison with the state-of-the-art in terms of number of model parameters (in millions), and % scores for mAP, per-class averages (CP, CR, CF1) and overall averages (OP, OR, OF1) for scene understanding datasets. Two settings are considered, *i.e.*, VOC → Clipart and Clipart → VOC. Best results are highlighted in **bold**.

Type	Method	# params	VOC → Clipart							Clipart → VOC						
			mAP	P_C	R_C	F_C	P_O	R_O	F_O	mAP	P_C	R_C	F_C	P_O	R_O	F_O
MLIC	ResNet101 [10]	42.5	38.0	64.8	14.3	22.5	82.3	18.3	29.9	50.1	66.2	17.5	25.5	83.9	29.6	43.7
	ML-GCN [5]	44.9	43.5	62.5	20.3	28.4	86.6	27.8	42.1	43.1	57.9	21.0	26.8	73.5	30.6	43.2
	ML-AGCN [26]	36.6	53.7	75.5	35.5	44.4	79.1	39.9	53.1	38.0	45.5	25.1	28.2	61.8	36.6	45.9
	ASL (TResNetM) [21]	29.4	56.8	72.0	38.5	47.6	82.8	45.7	58.9	64.2	69.0	30.7	37.3	80.0	45.7	58.2
Disc.-based	DANN (TResNetM+ASL) [9]	**29.4**	47.0	77.0	22.0	32.5	86.8	23.6	37.1	67.0	76.8	23.3	32.6	**93.1**	20.4	33.4
	DA-MAIC (TResNetM+ASL) [15]	36.6	**62.3**	77.4	**42.6**	**51.6**	83.1	**51.0**	**63.2**	74.3	84.5	**53.9**	**63.0**	83.7	**57.7**	**68.3**
Disc.-free	DALN (TResNetM+ASL) [4]	**29.4**	45.0	82.2	21.4	32.6	**92.0**	22.7	36.4	66.7	78.3	22.2	31.7	90.8	18.0	30.0
	DDA-MLIC (ours)	29.4	61.4	**84.7**	28.1	39.4	90.9	33.3	48.8	**77.0**	**86.9**	29.3	38.2	88.4	35.3	50.4

Table 4. Cross-weather domain shift: Comparison with the state-of-the-art in terms of number of model parameters (in millions), and % scores of mAP, per-class averages (CP, CR, CF1) and overall averages (OP, OR, OF1) for urban street datasets. Cityscapes → Foggy is the setting that is considered. Best results are highlighted in **bold**.

Type	Method	# params	Cityscapes → Foggy						
			mAP	P_C	R_C	F_C	P_O	R_O	F_O
MLIC	ResNet101 [10]	42.5	58.2	53.6	27.8	32.2	**93.2**	48.3	63.7
	ML-GCN [5]	44.9	56.6	56.1	34.6	38.8	89.4	56.9	69.6
	ML-AGCN [26]	36.6	60.7	60.1	48.3	50.9	81.7	**71.2**	**76.1**
	ASL (TResNetM) [21]	29.4	61.3	66.7	**50.8**	**53.8**	79.2	70.5	74.6
Disc.-based	DANN (TResNetM+ASL) [9]	**29.4**	53.5	50.6	12.5	18.6	89.5	21.8	35.1
	DA-MAIC (TResNetM+ASL) [15]	36.6	61.9	70.7	37.2	42.7	90.2	59.6	71.7
Disc.-free	DALN (TResNetM+ASL) [4]	**29.4**	54.8	56.8	19.5	25.4	90.2	33.8	49.2
	DDA-MLIC (ours)	29.4	**62.3**	**73.7**	45.7	48.9	84.1	69.3	76.0

forms discriminator-based DA approaches for MLIC [9, 15] on cross-sensor and cross-weather domain shift settings in terms of mAP. This observation was not consistent for sim2Ream domain shift, where our approach recorded an mAP improvement of 2.7% over other discriminator-based approaches on Clipart → VOC setting, but was slightly outperformed with 0.9% in terms of mAP by DA-MAIC [15] on VOC → Clipart setting.

Finally, we compare our method to the discriminator-free method proposed in [4] for single-label DA and adapted to MLIC as stated in Section 4.3. Unsurprisingly, our method consistently outperforms the adapted version of DALN for MLIC on all settings, reaching an improvement of more than 17% in terms of mAP on the AID → DFC scheme.

4.5.2 Qualitative analysis

The proposed DDA-MLIC is qualitatively compared with DANN [9] and DALN [4] in Figure 5 for the Clipart → VOC setting. The top row shows input images with their respective ground truth. The next three rows show the correct, incorrect, and missing predictions, in green, red, and blue, respectively. It can be noted that the proposed approach correctly predicts the labels of the five image samples, in contrast to other DA methods that are failing in some cases.

4.6. Ablation study

The results of the ablation study are shown in Table 5. We report the obtained mAP for the following settings, *i.e.*, AID → UCM, UCM → AID, UCM → AID, UCM → DFC,

VOC → Clipart and Clipart → VOC. The first row shows the mAP obtained in the absence of any domain adaptation strategy. The second row includes the scores obtained when adopting an adversarial domain adaptation approach using a standard domain discriminator. The third and last rows show the obtained results when using the proposed approach using a 2-Wasserstein distance. It can be clearly seen that by leveraging the classifier as a discriminator, the classification performance is generally improved in the presence of a domain shift.

4.7. Sensitivity analysis

In Table 8, we compare the mAP scores obtained for the cross-sensor domain shift, using different combinations of α_1 and α_2 defined in Eq. (5). We can observe from these results that giving either the same weights to each component or a slightly larger weight to the first component (negative labels) results in better performance.

4.8. GMM versus k-means

We employ the popular non-probabilistic clustering technique known as k-means to compare with the used GMM-based clustering. In contrast to the former, which uses hard thresholding to assign data points to specific clusters, GMM uses soft thresholding by maximizing the likelihood that any given data point will be in a given cluster. Table 7 compares the mAP scores obtained using the two methods. It can be clearly seen that using k-means results in a significant performance drop for all benchmarks.

Figure 5. Qualitative analysis: Comparison of the proposed DDA-MLIC (OURS) with DANN [9] and DALN [4] in terms of multi-label predictions on Clipart → VOC.

Table 5. Ablation study (w/o: without, w/: with). The reported % scores are mAP.

Methods	AID→UCM	UCM→AID	AID→DFC	UCM→DFC	VOC→Clipart	Clipart→VOC
Ours	63.24	54.87	62.13	70.64	61.44	76.96
Ours w/o DA	55.45 (-7.79)	54.12 (-0.75)	56.09 (-6.04)	68.91 (-1.73)	56.78 (-4.66)	64.15 (-12.81)
Ours w/ Discr.	52.54 (-10.70)	51.60 (-3.27)	51.60 (-10.53)	64.06 (-6.58)	46.97 (-14.47)	67.03 (-9.93)

Table 6. mAP comparison of using KL-divergence and 1-Wasserstein (1W) distance as discrepancy for domain alignment.

Methods	AID→UCM	UCM→AID	AID→DFC	UCM→DFC	VOC→Clipart	Clipart→VOC
Ours	63.24	54.90	62.13	70.64	61.44	76.96
Ours (with KL)	56.44 (-6.80)	53.51 (-1.39)	53.17 (-8.96)	64.55 (-6.08)	52.62 (-8.82)	77.86 (+0.90)
Ours (with 1W)	53.60 (-9.64)	53.20 (-1.70)	57.80 (-4.33)	69.70 (-0.94)	60.50 (-0.94)	75.50 (-1.46)

Table 7. mAP comparison of the proposed EM-based GMM clustering with k-means clustering.

Methods	AID→UCM	UCM→AID	AID→DFC	UCM→DFC	VOC→Clipart	Clipart→VOC
Ours	63.24	54.90	62.13	70.64	61.44	76.96
Ours (with k-means)	53.58 (-9.65)	52.20 (-2.70)	58.46 (-3.68)	68.06 (-2.57)	49.24 (-12.20)	68.27 (-8.69)

Table 8. Sensitivity analysis: A comparison of mAP by varying the values of regularizers for each GMM component on the aerial image datasets.

α values (α_1, α_2)	AID→UCM	UCM→AID	AID→DFC	UCM→DFC
α_1=0.1, α_2=0.9	56.0	50.6	55.4	67.1
α_1=0.2, α_2=0.8	55.0	52.4	55.3	67.4
α_1=0.3, α_2=0.7	56.0	50.3	57.0	69.3
α_1=0.4, α_2=0.6	58.0	52.4	59.2	69.3
α_1=0.5, α_2=0.5	**63.0**	53.0	57.7	**70.6**
α_1=0.6, α_2=0.4	54.4	**54.4**	55.4	66.4
α_1=0.7, α_2=0.3	54.9	52.6	57.6	65.6
α_1=0.8, α_2=0.2	53.8	52.9	**62.1**	69.3
α_1=0.9, α_2=0.1	55.6	53.9	56.0	66.6
α_1=1.0, α_2=0.0	57.8	52.0	57.2	69.5

4.9. Distance and divergence measure analysis

We propose using the 2-Wasserstein (denoted as 2W) distance as a discrepancy measurement for the learned GMM source and target components. As shown in Table 6, we compute the mAP scores using the popular KL-divergence and 1-Wasserstein (1W) distance in lieu of 2W. The effectiveness of the 2W distance as compared to other measures in the proposed method, given its continuity and differentiability properties, is clearly visible in Table 6. More specifically, using the KL divergence or the

1-Wasserstein distance as a discrepancy measure results in a slight to significant reduction in mAP across all benchmarks, ranging from 0.9% to 9.6%.

5. Conclusion

In this paper, a discriminator-free UDA approach for MLIC has been proposed. In contrast to existing methods which use an additional discriminator that is trained adversarially, our method leverages the task-specific classifier for implicitly discriminating between source and target domains. This strategy is proposed to avoid decoupling the classification and the discrimination tasks, while reducing the number of required network parameters. To achieve this, the adversarial loss has been redefined using a Féchet distance between the corresponding GMM components estimated from the classifier probability predictions. We have demonstrated that the proposed approach achieves state-of-the-art results on seven datasets covering three possible areas of domain shift, while considerably decreasing the size of the network. In future works, we will investigate a differentiable strategy for fitting the GMM for a fully end-to-end training of the network.

References

[1] Martin Arjovsky, Soumith Chintala, and Léon Bottou. Wasserstein generative adversarial networks. In *International conference on machine learning*, pages 214–223. PMLR, 2017. 4

[2] Sean Bell, C Lawrence Zitnick, Kavita Bala, and Ross Girshick. Inside-outside net: Detecting objects in context with skip pooling and recurrent neural networks. In *CVPR*, pages 2874–2883, 2016. 1

[3] Bindita Chaudhuri, Begüm Demir, Subhasis Chaudhuri, and Lorenzo Bruzzone. Multilabel remote sensing image retrieval using a semisupervised graph-theoretic method. *IEEE Transactions on Geoscience and Remote Sensing*, 56(2):1144–1158, 2017. 2, 3, 4, 5

[4] Lin Chen, Huaian Chen, Zhixiang Wei, Xin Jin, Xiao Tan, Yi Jin, and Enhong Chen. Reusing the task-specific classifier as a discriminator: Discriminator-free adversarial domain adaptation. In *CVPR*, pages 7181–7190, 2022. 1, 2, 3, 4, 6, 7, 8

[5] Zhao-Min Chen, Xiu-Shen Wei, Peng Wang, and Yanwen Guo. Multi-label image recognition with graph convolutional networks. In *CVPR*, pages 5177–5186, 2019. 5, 6, 7

[6] Marius Cordts, Mohamed Omran, Sebastian Ramos, Timo Rehfeld, Markus Enzweiler, Rodrigo Benenson, Uwe Franke, Stefan Roth, and Bernt Schiele. The cityscapes dataset for semantic urban scene understanding. In *CVPR*, pages 3213–3223, 2016. 5

[7] DC Dowson and BV Landau. The fréchet distance between multivariate normal distributions. *Journal of multivariate analysis*, 12(3):450–455, 1982. 2, 4

[8] Mark Everingham, Luc Van Gool, Christopher KI Williams, John Winn, and Andrew Zisserman. The pascal visual object classes (voc) challenge. *International journal of computer vision*, 88(2):303–338, 2010. 1, 5

[9] Yaroslav Ganin, Evgeniya Ustinova, Hana Ajakan, Pascal Germain, Hugo Larochelle, François Laviolette, Mario Marchand, and Victor Lempitsky. Domain-adversarial training of neural networks. *JMLR*, 17(1):2096–2030, 2016. 2, 6, 7, 8

[10] Kaiming He, Xiangyu Zhang, Shaoqing Ren, and Jian Sun. Deep residual learning for image recognition. In *CVPR*, pages 770–778, 2016. 1, 5, 6, 7

[11] Yuansheng Hua, Lichao Mou, and Xiao Xiang Zhu. Recurrently exploring class-wise attention in a hybrid convolutional and bidirectional lstm network for multi-label aerial image classification. *ISPRS journal of photogrammetry and remote sensing*, 149:188–199, 2019. 5

[12] Yuansheng Hua, Lichao Mou, and Xiao Xiang Zhu. Relation network for multilabel aerial image classification. *IEEE Transactions on Geoscience and Remote Sensing*, 58(7):4558–4572, 2020. 2, 3, 4, 5

[13] Naoto Inoue, Ryosuke Furuta, Toshihiko Yamasaki, and Kiyoharu Aizawa. Cross-domain weakly-supervised object detection through progressive domain adaptation. In *Proceedings of the IEEE conference on computer vision and pattern recognition*, pages 5001–5009, 2018. 5

[14] Yining Li, Chen Huang, Chen Change Loy, and Xiaoou Tang. Human attribute recognition by deep hierarchical contexts. In *ECCV*, pages 684–700. Springer, 2016. 1

[15] Dan Lin, Jianzhe Lin, Liang Zhao, Z Jane Wang, and Zhikui Chen. Multilabel aerial image classification with unsupervised domain adaptation. *IEEE Transactions on Geoscience and Remote Sensing*, 60:1–13, 2021. 2, 3, 5, 6, 7

[16] Tsung-Yi Lin, Michael Maire, Serge Belongie, James Hays, Pietro Perona, Deva Ramanan, Piotr Dollár, and C Lawrence Zitnick. Microsoft coco: Common objects in context. In *ECCV*, pages 740–755. Springer, 2014. 1

[17] Mingsheng Long, Yue Cao, Jianmin Wang, and Michael Jordan. Learning transferable features with deep adaptation networks. In *International conference on machine learning*, pages 97–105. PMLR, 2015. 2

[18] Mingsheng Long, Zhangjie Cao, Jianmin Wang, and Michael I Jordan. Conditional adversarial domain adaptation. *NeuRIPS*, 31, 2018. 2

[19] Zhongyi Pei, Zhangjie Cao, Mingsheng Long, and Jianmin Wang. Multi-adversarial domain adaptation. In *AAAI*, 2018. 2

[20] Duc Duy Pham, SM Koesnadi, Gurbandurdy Dovletov, and Josef Pauli. Unsupervised adversarial domain adaptation for multi-label classification of chest x-ray. In *ISBI*, pages 1236–1240. IEEE, 2021. 2

[21] Tal Ridnik, Emanuel Ben-Baruch, Nadav Zamir, Asaf Noy, Itamar Friedman, Matan Protter, and Lihi Zelnik-Manor. Asymmetric loss for multi-label classification. In *ICCV*, pages 82–91, 2021. 1, 3, 5, 6, 7

[22] Tal Ridnik, Hussam Lawen, Asaf Noy, Emanuel Ben Baruch, Gilad Sharir, and Itamar Friedman. Tresnet: High performance gpu-dedicated architecture. In *WACV*, pages 1400–1409, 2021. 1, 2, 3, 4, 5, 6

[23] Kuniaki Saito, Kohei Watanabe, Yoshitaka Ushiku, and Tatsuya Harada. Maximum classifier discrepancy for unsupervised domain adaptation. In *CVPR*, pages 3723–3732, 2018. 2

[24] Christos Sakaridis, Dengxin Dai, and Luc Van Gool. Semantic foggy scene understanding with synthetic data. *International Journal of Computer Vision*, 126:973–992, 2018. 5

[25] Jing Shao, Kai Kang, Chen Change Loy, and Xiaogang Wang. Deeply learned attributes for crowded scene understanding. In *CVPR*, pages 4657–4666, 2015. 1

[26] Inder Pal Singh, Enjie Ghorbel, Oyebade Oyedotun, and Djamila Aouada. Multi label image classification using adaptive graph convolutional networks (ml-agcn). In *2022 IEEE ICIP*, pages 1806–1810. IEEE, 2022. 6, 7

[27] Indel Pal Singh, Enjie Ghorbel, Oyebade Oyedotun, and Djamila Aouada. Multi-label image classification using adaptive graph convolutional networks: from a single domain to multiple domains. *arXiv preprint arXiv:2301.04494*, 2023. 2

[28] Inder Pal Singh, Nesryne Mejri, van Dat Nguyen, Enjie Ghorbel, and Djamila Aouada. Multi-label deepfake classification. In *IEEE Workshop on Multimedia Signal Processing*, 2023. 1

[29] Inder Pal Singh, Oyebade Oyedotun, Enjie Ghorbel, and Djamila Aouada. Iml-gcn: Improved multi-label graph convolutional network for efficient yet precise image classification. In *AAAI-W: Deep learning on graphs*, 2022. 1

[30] Gui-Song Xia, Jingwen Hu, Fan Hu, Baoguang Shi, Xiang Bai, Yanfei Zhong, Liangpei Zhang, and Xiaoqiang Lu. Aid: A benchmark data set for performance evaluation of aerial scene classification. *IEEE Transactions on Geoscience and Remote Sensing*, 55(7):3965–3981, 2017. 5

[31] Yi Yang and Shawn Newsam. Bag-of-visual-words and spatial extensions for land-use classification. In *Proceedings of the 18th SIGSPATIAL international conference on advances in geographic information systems*, pages 270–279, 2010. 5